Renewable Energy 256 (2026) 124188

Contents lists available at ScienceDirect

Renewable Energy

journal homepage: www.elsevier.com/locate/renene

Optimising the power regeneration and chemical oxygen demand removal in microbial fuel cell systems using integrated soft computing methods and multiple-objective optimisation

Mohammad Reza Chalak Qazani [a,b], Mostafa Ghasemi [c,d,**], Houshyar Asadi [e,*]

[a] College of Science and Engineering, James Cook University, Townsville, QLD, 4814, Australia
[b] Faculty of Computing and Information Technology, Sohar University, Sohar, 311, Oman
[c] Yangtze Delta Region Institute (Huzhou), University of Electronic Science and Technology of China, Huzhou, 313001, China
[d] Chemical Engineering Section, Faculty of Engineering, Sohar University, Sohar, 311, Oman
[e] Institute for Intelligent Systems Research and Innovation (IISRI), Deakin University, Geelong, VIC, 33216, Australia

ARTICLE INFO

Keywords:
Biological wastewater
Microbial fuel cell
Integrated soft computing
Deep learning

ABSTRACT

Microbial fuel cells (MFCs) have recently emerged as a sustainable technology for simultaneously treating wastewater and generating electricity. However, optimising their operational parameters to enhance performance remains a complex challenge. This study proposes an integrated framework that combines advanced machine learning models—long short-term memory (LSTM) and gated recurrent unit (GRU)—with a multi-objective genetic algorithm (MOGA) to optimise chemical oxygen demand (COD) removal and power output. Experimental data were obtained by varying glucose concentrations (1–9 g/L), yeast extract concentrations (1–5 g/L), and aeration rates (0–110 mL/min). Among the models evaluated, the LSTM model performed best in predicting COD removal. In contrast, the GRU model outperformed the others in power prediction. These surrogate models were incorporated into the MOGA to identify nine Pareto-optimal solutions. Experimental validation confirmed the high accuracy of the proposed approach, with average errors of 5.47 % for COD and 3.29 % for power. This work offers a cost-effective and scalable optimisation strategy, significantly reducing the need for exhaustive experimental trials while improving the efficiency and applicability of MFCs in real-world scenarios.

Nomenclature

Symbols:	
Bi-LSTM	Bi-directional Long Short-Term Memory
CC	Correlation Coefficient
CE	Coulombic Efficiency
COD	Chemical Oxygen Demand
DT	Decision Tree
GRU	Gated Recurrent Unit
ISC	Integrated Soft Computing
LSTM	Long Short-Term Memory
MFC	Microbial Fuel Cell
MLP	Multi-Layer Perceptron
MOO	Multi-Objective Optimisation
MSE	Mean Square Error
NRMSE	Normalised Root Mean Square Error
ORR	Oxygen Reduction Reaction
R2	R-square
RMSE	Root Mean Square Error
SEM	Scanning Electron Microscopy
StD	Standard Deviation
Acronyms:	
$\boldsymbol{b}$	number of electrons transferred per mole of oxygen
$\boldsymbol{f_t^j}$	Forget gates regulate memory retention
$\boldsymbol{F}$	Faraday constant
$\mathbf{h}_t$	Hidden state update at time t
$\widehat{\boldsymbol{h}}_t$	Candidate state
$\boldsymbol{i_t^j}$	Input gates regulate memory retention
$\boldsymbol{I}$	Current
$\boldsymbol{M}$	Molecular weight of oxygen
$\boldsymbol{n_{xi}}$	Normalised input data for the i^{th} entry
$\boldsymbol{R}$	External Resistance
$\boldsymbol{V}$	Voltage
$\boldsymbol{V_{an}}$	Volume of the anode chamber

(continued on next column)

(continued)

(continued on next page)

* Corresponding author.
** Corresponding author. Yangtze Delta Region Institute (Huzhou), University of Electronic Science and Technology of China, Huzhou, 313001, China.
E-mail addresses: mbaboli@csj.uestc.edu.cn (M. Ghasemi), houshyar.asadi@deakin.edu.au (H. Asadi).

https://doi.org/10.1016/j.renene.2025.124188
Received 20 June 2024; Received in revised form 1 July 2025; Accepted 7 August 2025
Available online 9 August 2025

(*continued*)

$\underline{x}$	Minimum values within the dataset
$\overline{x}$	Maximum values within the dataset
$y_i(n)$	Output of the previous neuron
z_t	Update gate
η	Learning rate
$\nu_i(n)$	Local induced field

1. Introduction

Addressing the global challenges of providing clean water and ensuring a sustainable energy supply is paramount. Both water scarcity and climate change pose significant threats to life on Earth. The rapid global population increase and improvements in living standards have escalated the strain on existing water and energy resources [1–3]. Additionally, the pervasive influence of global capitalism has led to heightened resource consumption. It has been predicted that in less than 5 decades, almost 30 % of the global population may have no access to clean water. Also, around 13 % of the global population won't have access to electricity [4,5]. The environmentally friendly energy sources have been seen as a new urgent demand by governments to minimise environmental impact. Microbial fuel cells (MFCs) are a new technology that can reduce environmental pollution from carbon dioxide emissions and treat wastewater. MFCs produce electricity through the reaction of microorganisms using the wastewater substance, including carbon and nitrogen. They are an effective and sustainable energy source [6].

Furthermore, MFCs present an environmentally friendly option as they are renewable energy resources that produce no carbon emissions. Even in comparison to processes such as treatment plants, MFCs do not consume large amounts of energy. In MFCs, the chemical oxygen demand (COD) removal is also carried out by electroactive bacteria, which oxidise organic compounds, hydrogen ions, free electrons, and protons to the electrode, serving as the electron acceptor [7,8]. Several types of microorganisms are involved in the operation of MFCs, and these microorganisms contribute to electricity generation through their participation in biochemical processes. The biofilm facilitates electron transfer via pili or conductive nanowires to the anode. Various factors affect the efficiency of MFCs, such as electrode material, separator, and catalyst. The most important factor is the medium that provides nutrients for microorganisms, which in turn determines the generation of bioelectricity and the effectiveness of wastewater treatment [9,10]. Research by Ji et al. [11] has demonstrated the capability of MFCs in removing per- and polyfluoroalkyl substances in integrated wetland systems. However, these substances harmed nitrogen removal and electricity production. More recently, Ullah [12] demonstrated that photosynthetic MFC using untreated domestic wastewater as a catholyte performs better in wastewater treatment and energy recovery than wetland-treated wastewater. Ballestas et al. [13] evaluated plant MFC using native plants and low-cost substrates for renewable energy generation, demonstrating the potential for sustainable, cost-effective electricity production in remote areas.

Soft computing methodologies have recently been applied across various fields, including materials microstructure, renewable energy, and energy production [14–18]. Fang et al. [19] achieved the maximum coulombic efficiency and power density of an MFC using a hybrid model that combined uniform design, relevance vector machine, and genetic algorithm. Garg et al. [20] proposed a surrogate model, including multi-gene genetic programming, feedforward neural networks, and support vector regression, to predict the voltage based on temperature and ferrous sulphate concentrations. Chen et al. [21] proposed a hybrid model incorporating wavelet analysis, extreme learning machines, and genetic algorithms to predict proton exchange in MFCs of electric vehicles, utilising humidity, current, hydrogen pressure, and temperature as inputs. Kannan et al. [22] integrated Monte Carlo simulations with reduced regression models to quantify uncertainties in PEMFC operation across activation, ohmic, and concentration loss regions. It develops reduced regression models for accurate performance prediction, enhancing robust control strategy development and operational efficiency. Dwivedi et al. [23] reviewed current research on MFCs,

Table 1
Comparative analysis of key related works on MFC optimisation.

Authors/Year	Methodology	Input Parameters	Output/Target	Key Contribution
Fang et al. [19], 2013	RVM and GA for optimisation	COD level, operational conditions	Coulombic efficiency, power output	Integrated relevance vector machine and GA to optimise energy efficiency in MFCs.
Garg et al. [20], 2014	Multi-gene GP, SVR, FFNN for surrogate modelling	Temperature, $FeSO_4$, voltage	Output voltage	Built and benchmarked predictive surrogate models for fuel cell voltage with hybrid ML methods.
Chen et al. [21], 2019	Hybrid model: Wavelet + ELM + GA	Humidity, hydrogen pressure, load current	Output power	Provided real-time PEMFC performance prediction under fluctuating conditions.
Kannan et al. [22], 2020	Monte Carlo simulation with reduced regression models	Catalyst type, current density	PEMFC performance	Enabled uncertainty quantification in fuel cell simulations to support robust system design.
Coşgun et al. [24], 2021	Decision Trees and Rule Mining for Algae Biofuel	Nutrient levels, pH, and media composition	Biomass, lipid yield	Developed interpretable rules for algae cultivation to maximise renewable energy yield.
Dwivedi et al. [23], 2022	Comprehensive review of soft computing in MFCs	–	–	Identified trends and future directions in AI applications for MFC control and prediction.
Shahbeik et al. [26], 2022	Random Forest for sludge pyrolysis prediction	Sludge type, temperature, and retention time	Biochar yield, syngas composition	Developed a robust predictive model for optimising waste-to-energy recovery from sludge.
Ghasemi et al. [27], 2023	MLP and SVR models for MFC prediction	Glucose, resistance, temperature	Power density	Demonstrated that SVR provides superior prediction accuracy over MLP for MFC performance modelling.
Nguyen et al. [28], 2023	Comparative analysis using XAI and ML	Flow rate, concentration, pH, temperature	Power output	Applied explainable AI to improve interpretability and optimisation in membraneless MFCs.
Hossain et al. [29], 2023	Boosted SVR and Regression Tree for prediction	Membrane thickness, resistance, and anode area	Power generation	Demonstrated high accuracy in power prediction using boosted ML models.
Ballestas et al. [13], 2024	Experimental plant-based MFC setup	Native plant type, substrate type	Voltage output	Validated the feasibility of using native plants for low-cost renewable electricity generation in remote areas.
Ullah et al. [12], 2024	Comparative study of catholyte types in photosynthetic MFCs	Catholyte type (domestic vs treated), light exposure	COD removal, voltage	Provided that untreated wastewater improves energy and treatment efficiency in MFCs.
Pan et al. [31], 2024	GBRT with Evolutionary Optimisation for gasification	Biomass-coal ratio, temperature, equivalence ratio	H_2 concentration, syngas yield	Achieved improved H_2 yield through ML-driven optimisation in gasification processes applicable to MFCs.
Kebede et al. [30], 2024	Bi-LSTM + Attention + Autoencoder for PEMFC lifecycle	Voltage cycles, operational time	Remaining Useful Life (RUL)	Advanced deep learning model for predictive maintenance in fuel cell systems.
This study	Deep learning (LSTM & GRU) + MOGA optimisation	Glucose, Yeast Extract, Aeration	COD removal, Power output	Proposed and validated a novel surrogate-based multi-objective optimisation framework with <5.5 % error, reducing experimental costs.

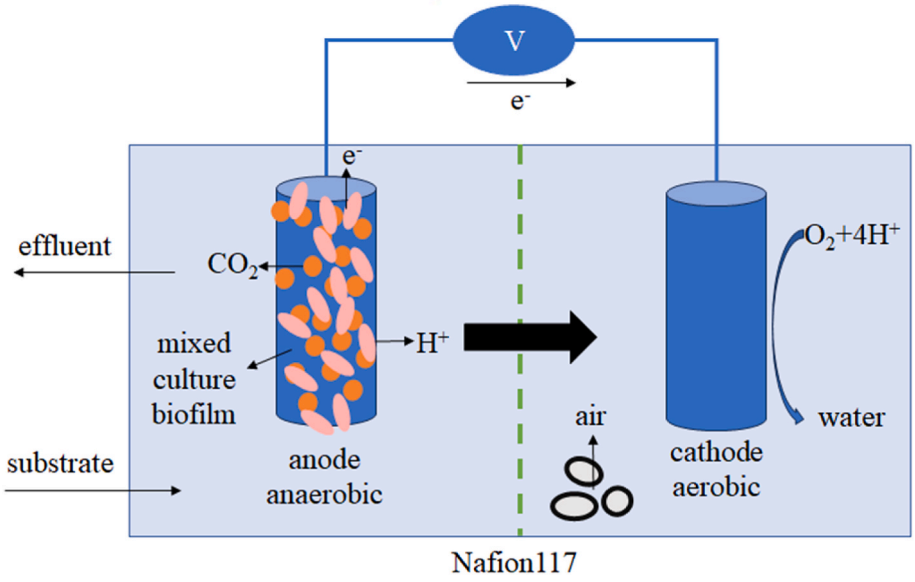

Fig. 1. The schematic structure of an MFC.

emphasising the role of soft computing techniques in enhancing their performance. Coşgun et al. [24] utilise decision trees and association rule mining to identify optimal microalgae conditions for high biomass and lipid production, facilitating efficient renewable biofuel production and guiding future experimental and industrial applications. Yang et al. [25] utilised gradient boost regression to model biomass microwave pyrolysis, effectively predicting product quantities (biochar, bio-oil, syngas). It demonstrates cost-effective and time-saving potential for optimising sustainable rural biorefineries. Shahbeik et al. [26] utilised random forest regression to accurately predict sludge pyrolysis product distribution, demonstrating the potential of soft computing methods to optimise bioenergy production from wastewater sludge while minimising experimental costs and labour.

Ghasemi et al. [27] significantly improved MFC performance predictions by employing a multi-layer perceptron with various hidden layers, resulting in a performance increase of 5.1819 compared to traditional support vector regression methods. Later, Ghasemi et al. [28] combined the fuzzy model with a salp swarm optimiser to enhance the efficiency of MFC in terms of power density, COD removal, and coulombic efficiency. Nguyen et al. [28] conducted a comparative analysis of multiple methods, including nine machine learning and three bio-inspired evolutionary algorithms. They discovered a higher efficiency of DT and particle swarm optimisation algorithms with a 239.024 % boost in power density. Hossain et al. [29] combined Bayesian optimisation with support vector regression. They boosted the regression tree to predict the MFC's power generation using membrane thickness, external resistance, and anode area as input operational parameters. Kebede et al. [30] use the transfer learning method by combining an autoencoder, bi-directional long short-term memory (Bi-LSTM), and attention mechanism to predict the remaining useful life of proton exchange MFC. Pan et al. [31] developed a gradient-boosting regression model. They employed an evolutionary algorithm to optimise biomass-coal co-gasification, enhancing syngas quality and identifying optimal parameters for maximum H_2 production and Fischer-Tropsch performance. To contextualise the novelty of the current work, Table 1 provides a comparative summary of key related studies, highlighting their methodologies, target outputs, and scientific contributions. This helps establish a clearer understanding of the current state of the art and underscores the unique aspects of the present study. This study addresses the existing research gap by proposing an integrated surrogate-based multi-objective optimisation framework for microbial fuel cells. It is hypothesised that combining deep learning models with genetic algorithms will enable accurate, experimentally validated predictions of COD removal and power generation while reducing the need for costly and time-intensive trials.

The main contribution of the following study can be divided into two main objectives:

1. The best surrogate models are generated to mitigate the functionality of the MFCs in terms of COD removal and power output, using operational parameters such as glucose, yeast extract, and aeration rate as inputs. Then, integrated soft computing (ISC) methods, including decision trees (DT), multi-layer perceptrons (MLP), gated recurrent units (GRU), and long short-term memory (LSTM) networks, are used to predict COD removal and power output in MFCs after the training processes of the models.
2. A multi-objective optimisation (MOO) using a genetic algorithm is employed to determine the optimal operational parameters (glucose, yeast extract, and aeration rate) that maximise COD removal and power output. It should be noted that the objective functions of the MOO are the two distinct ISC models, which were constructed to accurately predict COD removal and power output in the previous step.

The key contribution of this study is the development of a systematic hybrid model, combining ISC techniques and MOO, called ISC-MOO, which automatically extracts optimal solutions without the need for extensive practical testing, thereby reducing the time and cost of the process. In the first step, a comprehensive experimental study is designed using a full factorial mode to evaluate the effects of different input operational parameters on COD removal and power. This work represents the first comprehensive assessment of various ISC techniques applied to optimise the operational conditions of MFCs. The optimisation criteria, namely COD removal and power generation, were chosen because they represent the core performance metrics of MFC systems, directly correlating to wastewater treatment efficiency and renewable energy production.

The MFC process is analysed in detail in Section 2, which explains input operational parameters and the system's outputs. The experimental setup and data collection are also explained in this section. The proposed methodology, which utilises a hybrid of highly efficient ISC-MOO, is explained in detail in Section 3. Section 4 presents a detailed comparative analysis and discussion of the results obtained from the model, which was implemented using the MATLAB software. Lastly,

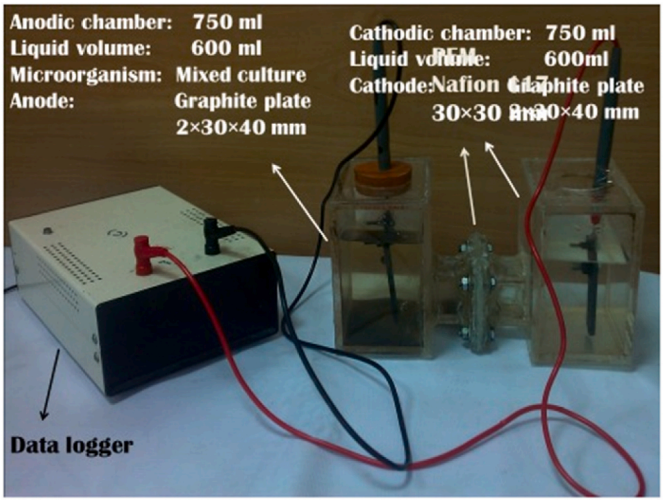

Fig. 2. The experiment setup for capturing the COD removal and power generation based on glucose, yeast extract, and aeration.

Table 2
Different levels of the input parameters for the design of the experiment.

Parameters	L1	L2	L3	L4	L5
Glucose (g/L)	1	3	5	7	9
Yeast Extract (g/L)	1	2	3	4	5
Aeration (mL/min)	0	20	50	80	110

Section 5 concludes the study by summarising and emphasising the key findings derived from the research.

2. Materials and Methods

2.1. Microbial fuel cell configuration

The structure of the MFC mirrors the design used in a prior study [32]. This MFC comprises two compartments separated by a proton exchange membrane, specifically Nafion 117. This highly selective membrane allows only protons to pass through to the anode. Electricity generation occurs via the oxygen reduction reaction (ORR) at the cathode electrode surface, with the voltage being monitored and recorded on a computer. Fig. 1 illustrates the schematic layout of the MFC.

2.2. Media and inoculation

Various concentrations of glucose (1–9 g/L) were used as the carbon source, while yeast extract in amounts ranging from 1 to 5 g/L served as the nitrogen source. The mineral and vitamin components were included as previously described. Nitrogen gas was flushed into the anode chamber for 15 min before the experiment to establish anaerobic conditions. An aquarium pump was used to supply air to the cathode chamber to facilitate the ORR. The media was inoculated with palm oil mill effluent from Selangor, which acted as anaerobic sludge in an anaerobic container. Before the operation, 10 ml of sludge was added to the media. The attached microorganisms were observed using scanning electron microscopy (SEM-Supra-55vp-Zeiss, Germany). The samples were dried and coated with a thin layer of gold before imaging. Fig. 2 illustrates the experimental setup used to measure COD removal and power generation, with varying glucose levels, yeast extract, and aeration levels. To ensure the highest accuracy of the system, a full factorial experimental design was employed, varying each input parameter as detailed in Table 2.

To conclude, the experiments were conducted at ambient temperature (25 ± 2 °C), with pH values maintained between 6.5 and 7.5 using a phosphate buffer. The electrode configuration, reactor volume (250 mL), and external resistance (1000 Ω) were kept constant throughout all trials. A full factorial design was employed with the following input parameter ranges: glucose (1–9 g/L), yeast extract (1–5 g/L), and aeration rate (0–110 mL/min).

2.3. Analysis and calculation

A voltammeter measured the generated voltage every second, with data being recorded and stored on a PC. The formulas below were used to calculate the current and power:

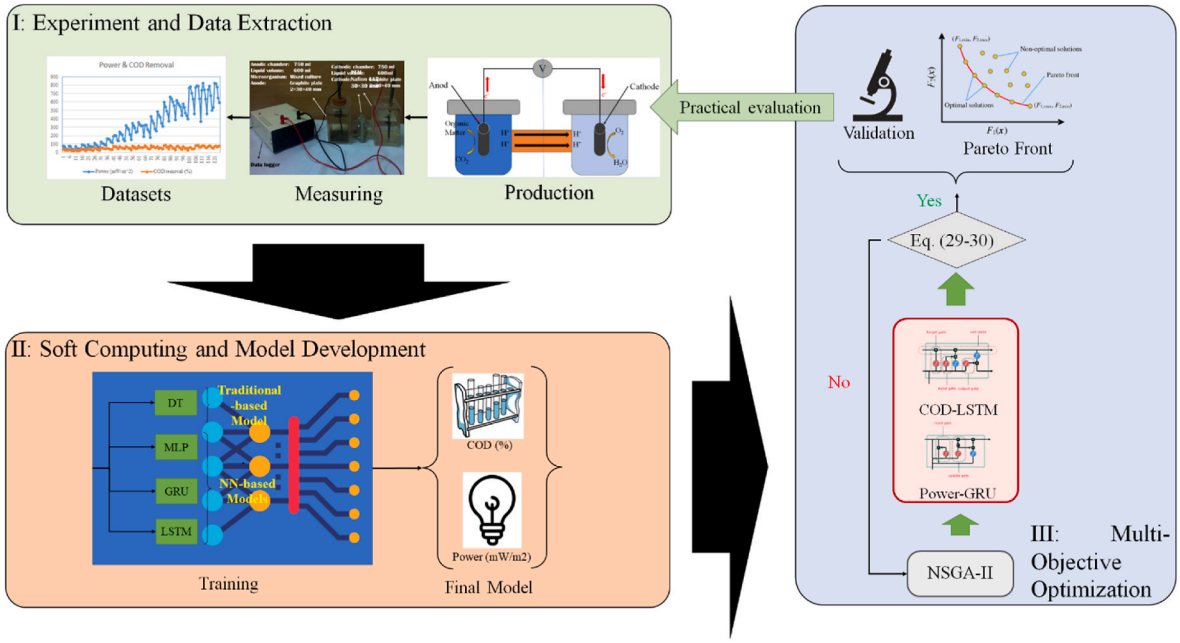

Fig. 3. The graphical introduction of the whole process in this research, including the practical experiment, ISC, and MOO/validation.

$$I = \frac{V}{R} \tag{1}$$

$$P = V \times I \tag{2}$$

where I represents the current, V denotes the voltage, and R is the external resistance.

The chemical solutions, which utilise high-range COD reagents, are used to determine the COD of MFCs. A sample was taken from the anode chamber and diluted ten times in water. Then, 2 mL of the diluted sample was added to high-range COD vials and heated to 150 °C. It should be noted that a spectrophotometer measures the COD levels [33]. The system's coulombic efficiency (CE) was calculated using the following formula:

$$CE = \frac{M \int_0^t I\, dt}{F\, b\, V_{an} \Delta COD} \tag{3}$$

where M, F, $b = 4$, ΔCOD, and V_{an} are the molecular weight of oxygen, Faraday constant, number of electrons transferred per mole of oxygen, change in COD, and volume of the anode chamber. Purging the nitrogen gas into the anode chamber for 10 min establishes anaerobic conditions. At the same time, the air pump supplied air to the cathode chamber, facilitating the ORR reaction.

2.4. Range of control parameters

The choice of control parameters —glucose concentration, yeast extract level, and aeration rate —was based on their well-documented impact on microbial action, substrate accessibility, and oxygen exchange in MFC frameworks. The glucose concentration (1–9 g/L) was chosen to represent the full range of natural stacking conditions commonly found in genuine wastewater streams, ensuring the relevance of the results to both residential and industrial effluents. Yeast extract (1–5 g/L) was chosen as a nitrogen source and microbial development enhancer at concentrations regularly utilised in MFC studies for biofilm development and electron exchange enhancement. The aeration rate (0–110 mL/min) was adjusted to simulate oxygen accessibility within the cathode, ranging from restricted to high oxygen exchange rates, as observed in field-scale wastewater treatment plants. These parameter ranges were also chosen to provide adequate flexibility for robust surrogate model preparation and to ensure that the optimised arrangements are relevant and adaptable for real-world MFC applications.

3. Simulation method

The schematic representation of the proposed method, ISC-MOO, is represented in Fig. 3, which comprises three main steps. It is used to enhance the efficiency of the MFC process in terms of COD removal and power outputs. Also, the optimisation framework developed in this study is flexible and can incorporate different input parameters specific to regional wastewater characteristics and resource availability, ensuring its global applicability.

In the first step, experiments are designed and conducted to extract datasets that connect the input operational parameters (glucose concentration, yeast extract, and aeration) to the outputs (COD removal and power generation). It consists of experiments, measurements, and the generation of datasets. The full factorial experimental design method ensures robustness in understanding process dynamics by generating a rich dataset.

In the second step, the surrogate models of MFC behaviour are developed using ISC methods, including DT, MLP, LSTM, and GRU. Each model is trained and evaluated to predict the system's outputs, including COD removal and power generation in MFC systems. Then, the models with the highest performance in predicting COD removal and power generation are selected as the best potential candidates for representing MFC behaviour.

In the third step, the selected predictive models from the second step are considered inside the MOO framework as objective functions. It is worth noting that the genetic algorithm is considered the most suitable method for representing MOO. As a result, the Pareto-optimal set of operating conditions is extracted to balance the MFC application's maximum COD removal and power generation. The extracted optimal input operational parameters offer valuable insights for enhancing the MFC performance. The numerical surrogate models (LSTM and GRU) were trained using data generated from the full factorial experimental design. The models were constrained to operate within the same input bounds used experimentally. They assumed steady-state conditions with stable pH, temperature, and microbial activity.

However, the applicability of the proposed ISC-MOO cannot be approved without a practical evaluation of the extracted solution in this research. Then, the experiments were conducted using the extracted optimal input operational parameters to prove the effectiveness of our proposed methodology. It can assure the potential for widespread adoption in environmental engineering and sustainable energy production.

3.1. Preprocessing

The extracted dataset via the full factorial experiments cannot be used without implementing the preprocessing task. The most significant issue encountered during the data preprocessing of our model is the removal of outliers, as they can compromise the robustness of the developed model. In addition, other issues, such as irrelevancy, duplication, noise, and missing data, are considered and addressed in the dataset based on their presence.

In the next step, the normalisation process is implemented in the dataset to normalise the data distribution and reduce the computation load of the proposed ISC. The dataset can be normalised as follows:

$$n_{x_i} = \frac{x_i - \underline{x}}{\overline{x} - \underline{x}} \tag{4}$$

where n_{xi}, $\underline{x}$, and $\overline{x}$ are the normalised input data for the i^{th} entry, minimum, and maximum values within the dataset, respectively.

Also, the dataset is partitioned into 80 %, 10 %, and 10 % for training, validation, and testing, respectively. It ensures the integrity and generalizability of the developed models. This partitioning scheme ensures the model is rigorously evaluated on unseen data, enhancing its predictive capabilities and real-world applicability. The testing data are withheld from the network until the final testing stage, ensuring an unbiased assessment and reliable performance metrics for the proposed models.

3.2. Decision tree

DT is the first investigated model in this research as it has proven its efficiency in the data mining and analysis sectors [34]. DT can handle classification and regression problems based on the nature of the datasets. It can be considered a supervised learning method. The architecture of the DT is developed using nodes, branches, and leaves. Nodes are divided into two types: root and internal. The starting and decision-making points are specified using root and internal nodes. The branch is used to connect notes using arrows. They used to specify a potential decision and reaction inside the DT. The leaves, which are the furthest branches of the DT, extract the final outputs of the system. The most famous DT algorithms are CART, C4.5, and Chi-squared automatic interaction detection [35]. The higher regression capability of the CART algorithm, with no parameter dependency, was the primary motivation for choosing this method in this research.

3.3. Multi-layer perceptron

The MLP is an advanced form of feedforward neural network with multiple layers. It can be used for classification and regression problems based on the provided datasets. It can be considered a supervised learning method. During the training of MLP, the goal is to minimise the loss function by adjusting the network's parameters (weights and biases) using backpropagation. The weights are calculated using the gradient descent method as follows:

$$\Delta w_{ij}(n) = -\eta \frac{\partial \varepsilon(n)}{\partial \nu_i(n)} y_i(n) \tag{7}$$

where η, $y_i(n)$, and $\nu_i(n)$ are the learning rate, the output of the previous neuron, and the local induced field, respectively. The Levenberg-Marquardt learning method is employed to determine the weights of the MLP in this study [36].

3.4. Gated recurrent unit

The GRU is a modified version of a recurrent neural network that cooperates with gating mechanisms, which can handle time-series and analyse datasets [37]. GRU's architecture comprises the update gate, reset gate, and candidate activation vector. The update gate is responsible for retaining the previous hidden state and adding the amount of candidate activation to the new hidden state. The hidden state update at time t is extracted as follows:

$$h_t = (1 - z_t) \odot \widehat{h}_t + z_t \odot \widehat{h}_{t-1} \tag{14}$$

where $\widehat{h}_t$ and z_t represents the candidate state and update gate, respectively.

The reset gate determines whether to reset or forget the previous hidden state based on the current input. The candidate activation vector is calculated using a transformed version of the previous hidden state and the current input to be added to the memory of the GRU.

3.5. Long-short term memory

LSTM is an improved version of the recurrent neural network that uses a memory cell to solve the vanishing gradient problem. The architecture of LSTM is composed of the input, forget, and output gates. These gates add, remove, and output information from the memory cell. The existence of a memory cell is the primary reason for robust predictions across long sequences within an LSTM, as it retains the temporal states. The cell state is updated with the combination of previous and new memory values, as follows:

$$c_t^j = f_t^j c_{t-1}^j + i_t^j \widetilde{c}_t^j \tag{24}$$

where f_t^j and i_t^j are forget and input gates that regulate memory retention, respectively. Backpropagation through time and gradient descent are used for training and minimising the error within the loss function.

3.6. Multiple-objective genetic algorithm

The MOO-GA employs genetic algorithms to efficiently solve complex multi-objective problems. Integrating mutation and crossover techniques generates new populations iteratively, preserving optimal solutions via elitist strategies. The Pareto front is extracted in a single run, streamlining computational efficiency.

Objective functions in this study evaluate discrepancies between experimental and predicted values:

$$J_{\mathrm{COE}}(G, YE, A) = 100 - \frac{1}{n} \sum_{i=1}^{n} (COD_i - \widehat{COD}_i)^2 \tag{29}$$

$$J_{\mathrm{P}}(G, YE, A) = 1000 - \frac{1}{n} \sum_{i=1}^{n} (P_i - \widehat{P}_i)^2 \tag{30}$$

where COD and $\widehat{COD}$ are the actual and predicted chemical oxygen demand values, respectively. Also, P and $\widehat{P}$ are the actual and predicted chemical power generation, respectively. The optimisation seeks to maximise COD removal and power output.

While COD removal and power generation serve as critical performance metrics, the optimised solutions also demonstrate promising economic and environmental sustainability implications. For instance, reducing COD levels contributes to cost savings in wastewater treatment processes. At the same time, the power generated can offset energy consumption in industrial applications. Future work could include developing a multi-criteria decision-making framework that incorporates additional parameters, such as economic feasibility, scalability, and lifecycle environmental impact.

4. Results and discussions

This section is structured into four distinct subsections, each addressing crucial aspects of the experimental investigation. The initial subsection examines microbial colonisation patterns on the surface of electrodes, shedding light on the intricate dynamics of microorganism-electrode interactions. The subsequent subsection focuses on developing advanced computational models tailored to predict key performance metrics, namely COD removal and power generation. These models are meticulously trained and validated using data encompassing variations in glucose concentration, yeast extract, and aeration levels. In the following subsection, we embark on a detailed analysis of the influence of input parameters (glucose, yeast extract, and aeration) on the dynamic behaviour of the MFC system. Leveraging insights from the developed computational models, we unravel the complex relationships between input variables and system outputs, providing invaluable insights for process optimisation. Subsequently, attention shifts towards integrating predictive models within a multi-objective optimisation framework. The most adept computational models for predicting COD removal and power generation are seamlessly integrated into an MOO using a genetic algorithm to extract optimal operating conditions. Through iterative optimisation, using a genetic algorithm, the MOO identifies Pareto-optimal solutions that maximise system performance while balancing conflicting objectives. Concluding this section, the extracted optimal operating conditions are subjected to rigorous experimental validation to assess the efficacy and reliability of the proposed methodology. Real-world testing ensures the robustness and applicability of optimised operational parameters, affirming the efficacy of our approach in enhancing MFC performance. The surrogate models were developed under the assumption of steady-state MFC operation with spatial homogeneity, based on a well-mixed reactor design. Input parameters were bounded within experimentally tested ranges, and the models were designed to generalise only within this validated domain. Mechanistic reactions were not explicitly modelled, as the approach relies on empirical learning from experimental data.

4.1. Experimental methodology

The experimental methodology used to examine the performance of the Microbial Fuel Cell (MFC) system is described in detail in this section. The methodology encompasses the operational processes and MFC configuration, as well as the analytical techniques employed to evaluate performance, and the structured experimental design used to examine the impact of key operational parameters.

4.1.1. MFC set up and procedures

The experimental procedure was carried out utilising a dual-chamber MFC configuration, as previously outlined in the Materials and Methods

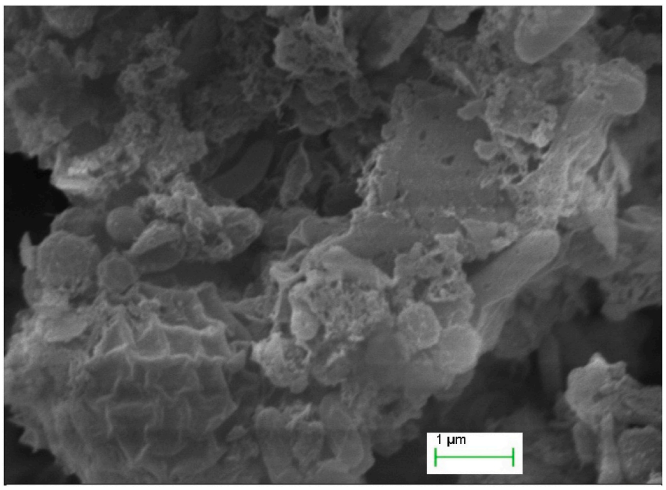

Fig. 4. The attachment of microorganisms on the electrode surface.

section. The two chambers were divided by a Nafion 117 proton exchange membrane to facilitate proton transfer. The anode chamber was maintained under anaerobic conditions by purging with nitrogen gas for 15 min before each experiment. Palm oil mill effluent sludge sourced from Selangor was employed as the microbial inoculum. Glucose (1–9 g/L) and yeast extract (1–5 g/L) were utilised as the sources of carbon and nitrogen, respectively. The cathode chamber was continuously aerated with an aquarium air pump to promote the oxygen reduction reaction (ORR). The reactor volume was maintained at 250 mL, with an external resistance set at 1000 Ω. The voltage across the electrodes was monitored and recorded in real-time using a digital voltmeter linked to a data acquisition system on a computer.

4.1.2. Measurement methods

A high-range COD testing technique was used to quantify COD elimination. Anode chamber samples were taken, diluted ten times, and then heated to 150 °C in COD digestion vials containing 2 mL of the diluted sample. After digestion, the COD concentration was measured with a spectrophotometer. The output voltage was continually recorded and monitored every second. The recorded voltage and the known external resistance were used to compute the current and power density. Using phosphate buffer solutions, the pH was maintained between 6.5 and 7. The studies were carried out at room temperature (25 ± 2 °C).

4.1.3. Experimental design and repeatability

A full factorial exploratory plan was utilised, resulting in 125 test runs to cover all combinations of glucose, yeast extract, and air circulation rate levels, as shown in Table 2. Each test was repeated three times, and the average value was used to create and prepare the surrogate models (LSTM for COD expulsion and GRU for the control era).

4.2. Biofilm

The attachment of microorganisms on the electrode surface is shown in Fig. 4. The photo shows thick layers of microorganisms attached to the electrode surface. The communities of microorganisms in the wastewater and the topography of the surface, as well as the affinity of the mixed cultures to the electrode surface, are the primary factors influencing the attachment of microorganisms to the electrode surface. The SEM photo reveals that the biofilm is composed of a rich mixture of Hyla, Proteobacteria, and Firmicutes, which thrive in the absence of oxygen and are rich in nutrients [27].

4.3. Modelling

Four ISC methods, DT, MLP, GRU, and LSTM, are individually trained using the extracted datasets to predict COD removal and power. It should be noted that the datasets are reported in the supplementary material, which consists of 125 sets (full factorial) of experiments based on the provided values in Table 2. To validate the results to extract the most efficient ISC methods, the correlation coefficient (CC), mean square error (MSE), root means square error (RMSE), normalised root mean square error (NRMSE), mean of error, standard deviation (StD), and R-square (R^2) are used in this study. The calculation of each validation parameter is mentioned in the Appendix Section. Table 3 presents the training and testing results for all datasets employed in the implemented ISC methods in this study, including DT, MLP, GRU, and LSTM, for calculating COD removal. The bold style is used to indicate the best-extracted parameter inside Table 3. In terms of CC, MSE, RMSE, NRMSE, Std, and R2, GRU and LSTM achieve better results during training, testing, and across all datasets than those of DT and MLP. It proves that GRU and LSTM are more efficient than DT and MLP. Additionally, it is worth noting that LSTM is more efficient in predicting COD removal than GRU. Then, COD-LSTM was selected as the most efficient method for predicting COD removal based on glucose, yeast extract, and aeration. As it is evident, LSTM defeats the GRU in point of CC (Training, testing, and all), MSE (training and all), RMSE (training and all), NRMSE (training and all), mean (testing), StD (training and all), and R^2 (Training, testing, and all).

Table 4 presents the training and testing results for all datasets employed in the implemented ISC methods in this study, including DT, MLP, GRU, and LSTM, for calculating power generation. During the training process, DT defeated the other ISC methods (MLP, GRU, and LSTM) in terms of MSE, RMSE, NRMSE, mean of error, StD, and R^2, based on the represented results in Table 3. Also, GRU was able to defeat the other ISC methods (DT, MLP, and LSTM) in terms of MSE, RMSE, NRMSE, mean of error, StD, and R^2, based on the represented results in Table 3 during the testing process. Furthermore, LSTM was able to

Table 3
The extracted results for investigation of implementing ISC methods (DT, MLP, GRU, and LSTM) for calculation of COD removal (%) based on glucose (g/L), yeast extract (g/L), and aeration (mL/min).

Method	Stage	CC	MSE	RMSE	NRMSE	Mean	StD	R^2
DT	Train	0.9156	31.90	5.65	0.11	$\mathbf{-3.20 \times 10^{-15}}$	5.68	0.8634
	Test	0.8215	182.47	13.51	0.30	2.64	13.52	0.5880
	All	0.8889	62.02	7.88	0.16	0.53	7.89	0.7798
MLP	Train	0.8323	86.89	9.32	0.18	3.01×10^{-1}	9.36	0.6386
	Test	0.7404	239.17	15.47	0.34	−1.39	15.72	0.2341
	All	0.8033	117.35	10.83	0.21	**−0.03**	10.88	0.5444
GRU	Train	0.8973	44.32	6.66	0.13	7.13e-1	6.65	0.8083
	Test	0.8719	**111.89**	**10.58**	**0.23**	0.80	**10.77**	0.7010
	All	0.8861	57.84	7.61	0.15	0.73	7.60	0.7813
LSTM	Train	**0.9471**	**18.79**	**4.45**	**0.09**	-1.86×10^{-1}	**4.47**	**0.9159**
	Test	**0.8742**	116.3	10.78	0.24	**0.55**	11.00	**0.7035**
	All	**0.9226**	**39.09**	**6.25**	**0.12**	−0.04	**6.28**	**0.8560**

Table 4
The extracted results for investigation of implementing ISC methods (DT, MLP, GRU, and LSTM) for calculation of power (mW/m^2) based on glucose (g/L), yeast extract (g/L), and aeration (mL/min).

Method	Stage	CC	MSE	RMSE	NRMSE	Mean	StD	R^2
DT	Train	0.9933	**544.90**	**23.34**	**0.07**	$\mathbf{2.27 \times 10^{-15}}$	**23.46**	**0.9904**
	Test	0.9735	2352.29	48.50	0.17	−3.95	49.34	0.9622
	All	0.9910	906.37	30.11	0.09	−0.79	30.22	0.9845
MLP	Train	0.9391	5062.91	71.15	0.21	−1.52	71.50	0.9092
	Test	0.9352	5118.68	71.54	0.25	14.10	71.59	0.9276
	All	0.9444	5074.07	71.23	0.21	1.61	71.50	0.9149
GRU	Train	0.9897	1348.77	36.73	0.11	3.49	36.74	0.9763
	Test	0.9729	**789.35**	**28.10**	**0.10**	**−1.68**	**28.62**	**0.9873**
	All	0.9890	1236.90	35.17	0.11	2.46	35.22	0.9788
LSTM	Train	**0.9953**	775.53	27.85	0.08	0.66	27.98	0.9862
	Test	**0.9806**	960.66	31.00	0.11	−2.70	31.51	0.9843
	All	**0.9941**	**812.56**	**28.51**	**0.09**	**−0.02**	**28.62**	**0.9859**

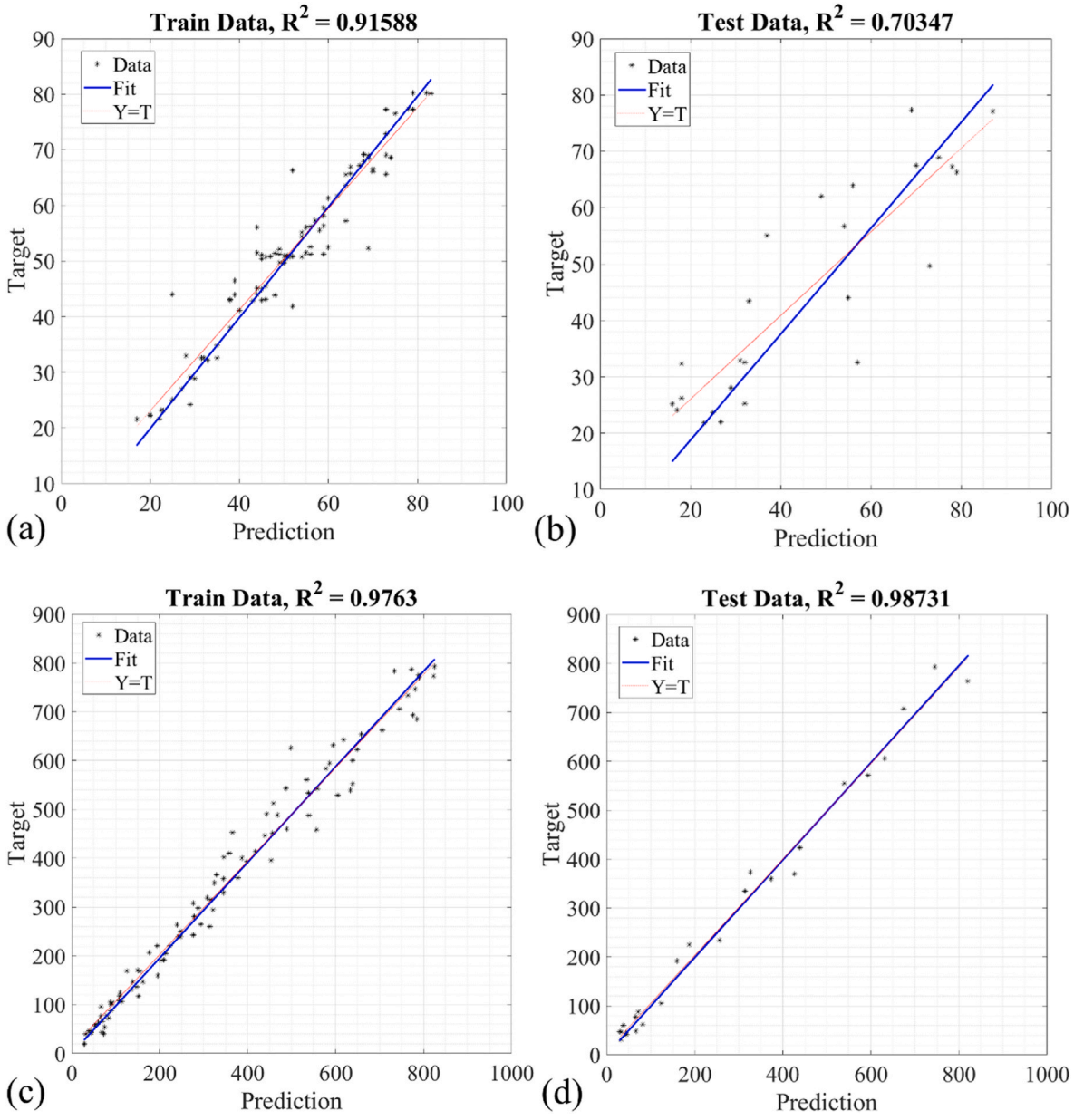

Fig. 5. The regression of the dataset (a) using COD-LSTM for prediction of the COD removal (%) with implementation of training data; (b) using COD-LSTM for prediction of the COD removal (%) with implementation of testing data; (c) using P-GRU for prediction of the power (mW/m^2) with implementation of training data; (d) using P-GRU for prediction of the power (mW/m^2) with implementation of testing data.

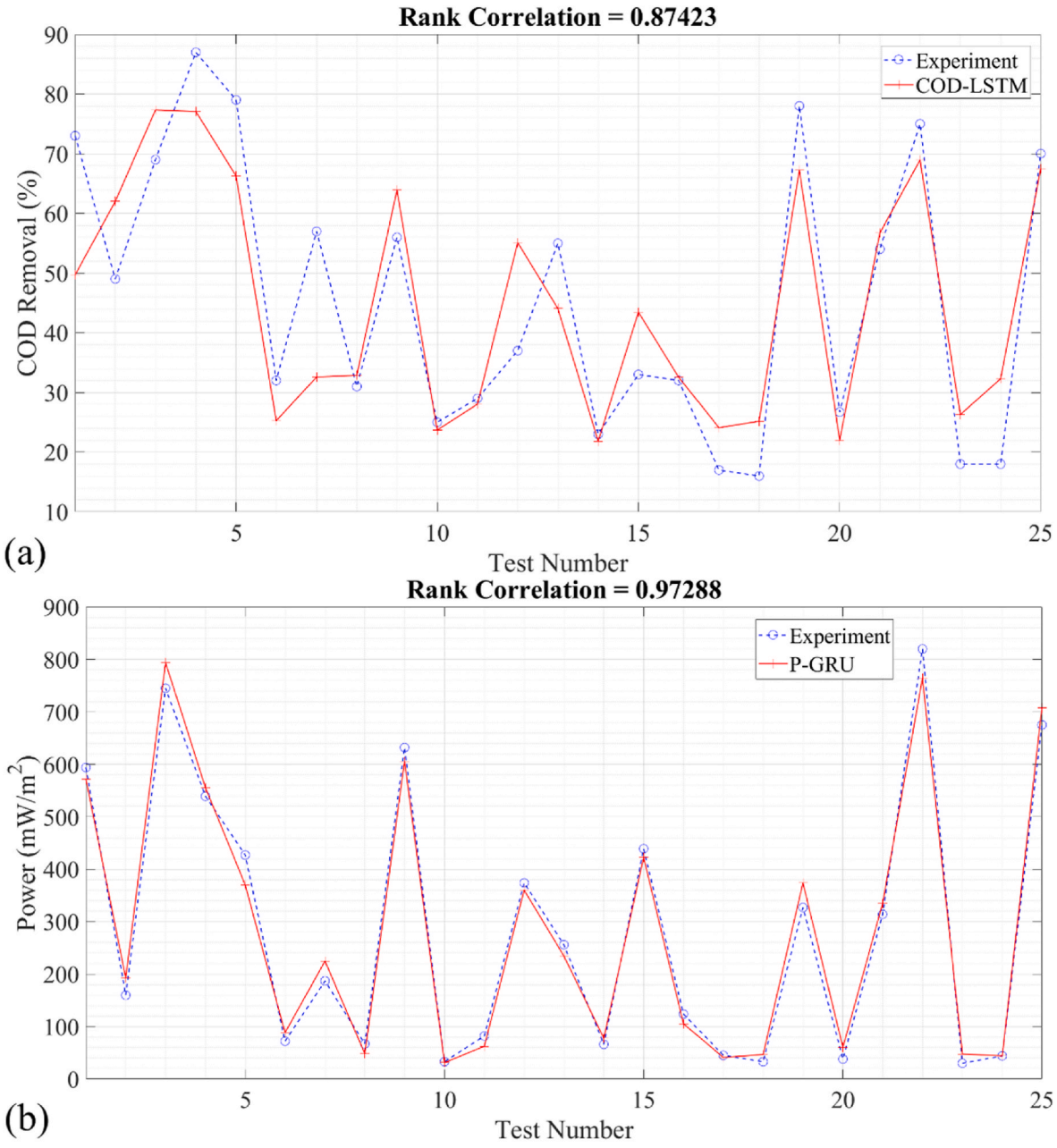

Fig. 6. The experimental and predicted outputs of the MFC process using (a) COD-LSTM for prediction of the COD removal (%); (b) P-GRU for prediction of the power (mW/m^2).

defeat the other ISC methods (DT, MLP, and LSTM) in terms of CC, MSE, RMSE, NRMSE, mean of error, StD, and R^2, based on the represented results in Table 3 during the implementation of all datasets (training and testing). As the testing process is the most critical part of evaluating the results, the GRU is chosen to predict power in the MFC process, and it is referred to as P-GRU.

The interplay between glucose and aeration significantly influenced COD removal, with optimal performance observed at a glucose concentration of 8.6 g/L and an aeration rate of 12.08 mL/min. These findings align with Shahbeik et al. [26], who demonstrated the critical role of substrate concentration in enhancing microbial activity and biofilm formation. However, our work extends this understanding by quantifying these relationships through machine learning models, offering a scalable framework for real-world applications.

As the COD-LSTM and P-GRU are the most efficient ISC methods in calculating COD removal and power, the results of these two investigated methods are analysed in the rest of the paper. Fig. 5a–d illustrate the correlations between the outcomes derived from the experimental study and the forecasts generated for COD removal using COD-LSTM and P-GRU during the training and testing dataset implementation, respectively. As indicated in Fig. 5a and b, the predictive performance of COD-LSTM in estimating COD removal exhibits R^2 values of 0.9159 and 0.7035 for the training and testing datasets, respectively. Similarly, Fig. 5c and d illustrate a distinct pattern, where R^2 for P-GRU in the domain of power prediction is 0.9763 and 0.9873 for the training and testing datasets, respectively.

Fig. 6a–b displays COD removal and power assessment within the MFC process during the testing process of the COD-LSTM and P-GRU, respectively. This appraisal involves employing both the experimental results and the suggested COD-LSTM and P-GRU models during the testing phase of the network. The experimental results serve as the benchmark against which the outcomes of COD-LSTM and P-GRU are

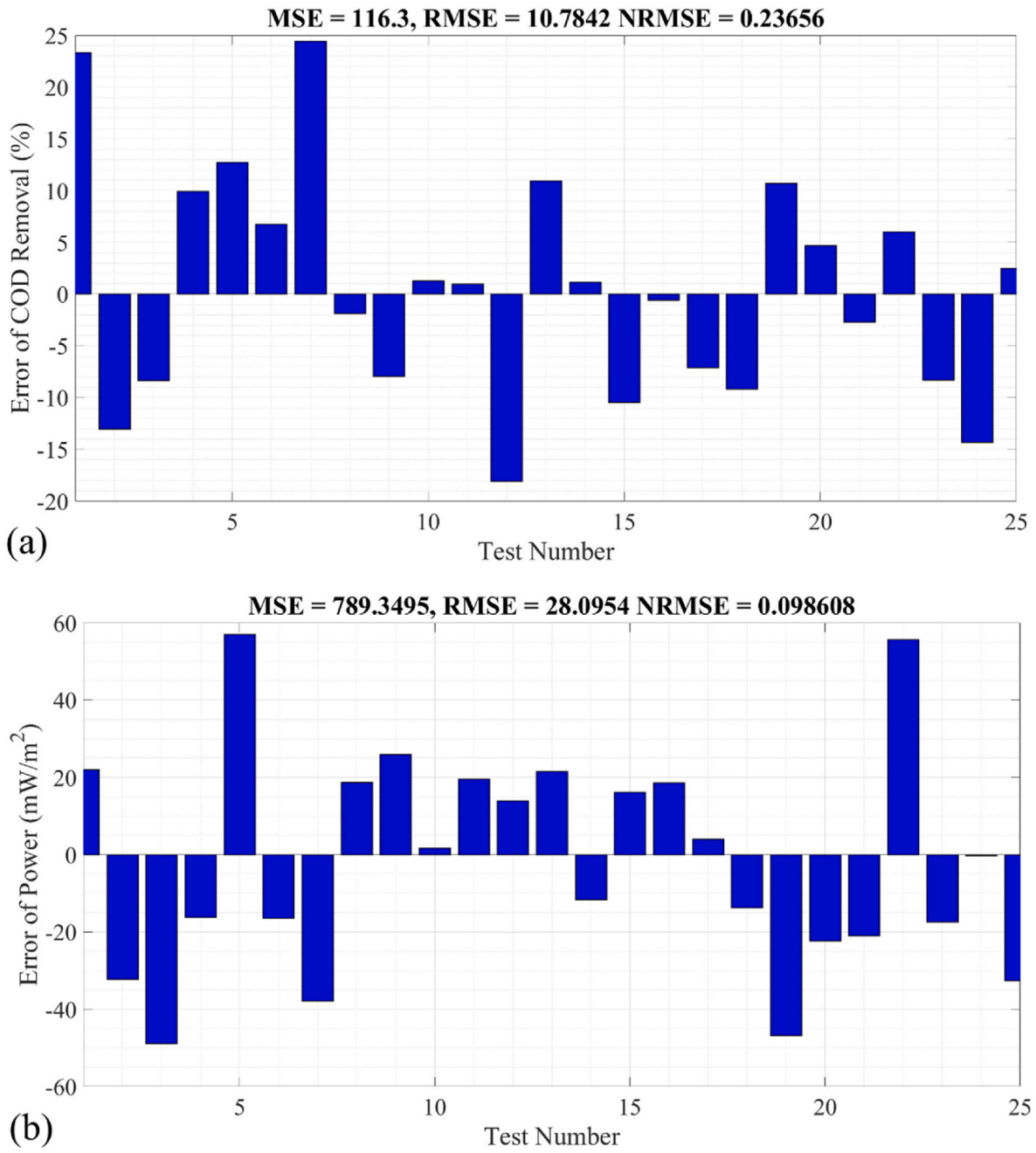

Fig. 7. The error between the experimentally captured and predicted value using the proposed T2FNN models to predict (a) COD removal (%); (b) power (mW/m^2).

juxtaposed, facilitating an evaluation of the proposed models' precision. Fig. 6a delineates the computation of COD removal for 25 testing samples, utilising both the experiment and COD-LSTM. As evidenced by the findings in Fig. 6a, the CC between the experimental outcomes and the extracted COD removal yielded by the proposed COD-LSTM model amounts to 0.8742. Furthermore, Fig. 6b demonstrates that encompassing 25 testing samples, the CC between the experimental results and the proposed P-GRU model's extracted power stands at 0.9729.

Fig. 7a and b illustrate the discrepancy between the anticipated and reference (experimental) values for COD removal and power predictions, employing the COD-LSTM and P-GRU. Analysing the outcomes depicted in Fig. 7a, it becomes evident that the MSE between the predicted and experimental COD removal, as determined by the proposed COD-LSTM, equates to 116.3 (%). Similarly, Fig. 7b shows that the MSE of the predicted and experimental power is 789.3 (mW/m^2). Additionally, the RMSE values for the predicted and experimentally recorded COD removal and power are 10.78 and 28.10, respectively, as shown in Fig. 7a–b. Lastly, assessing the NRMSE, it is deduced that P-GRU boasts superior predictive accuracy compared to COD-LSTM, given its lower value of 0.2366 compared to 0.0986 (Fig. 7a and b). An error analysis was performed using standard statistical metrics (MSE, RMSE, NRMSE), with the results summarised in Tables 3–4 and visually represented in Fig. 7. These metrics quantify the prediction error margins of the surrogate models in comparison to experimental observations.

4.4. *Influence of parameters*

Fig. 8a–c shows the rule surface of the extracted COD-LSTM in calculating the COD removal based on arrangements of the input process parameters, including glucose-aeration, glucose-yeast extract, and yeast extract-aeration, respectively. To be precise, Fig. 8a presents the variation of COD removal based on the variation of glucose (from 0 to 10 g/L)

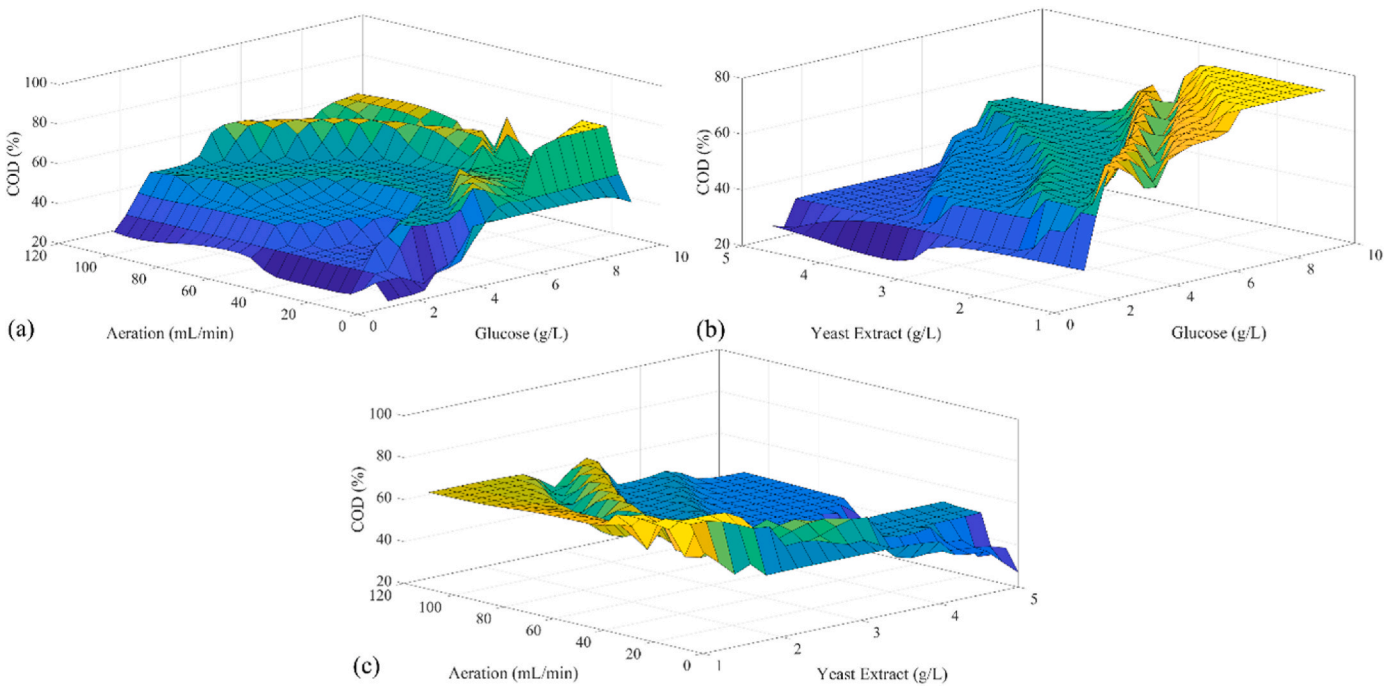

Fig. 8. COD-LSTM rule surface for calculation of COD removal (%) using (a) glucose-aeration; (b) glucose-yeast extract; (c) yeast extract-aeration.

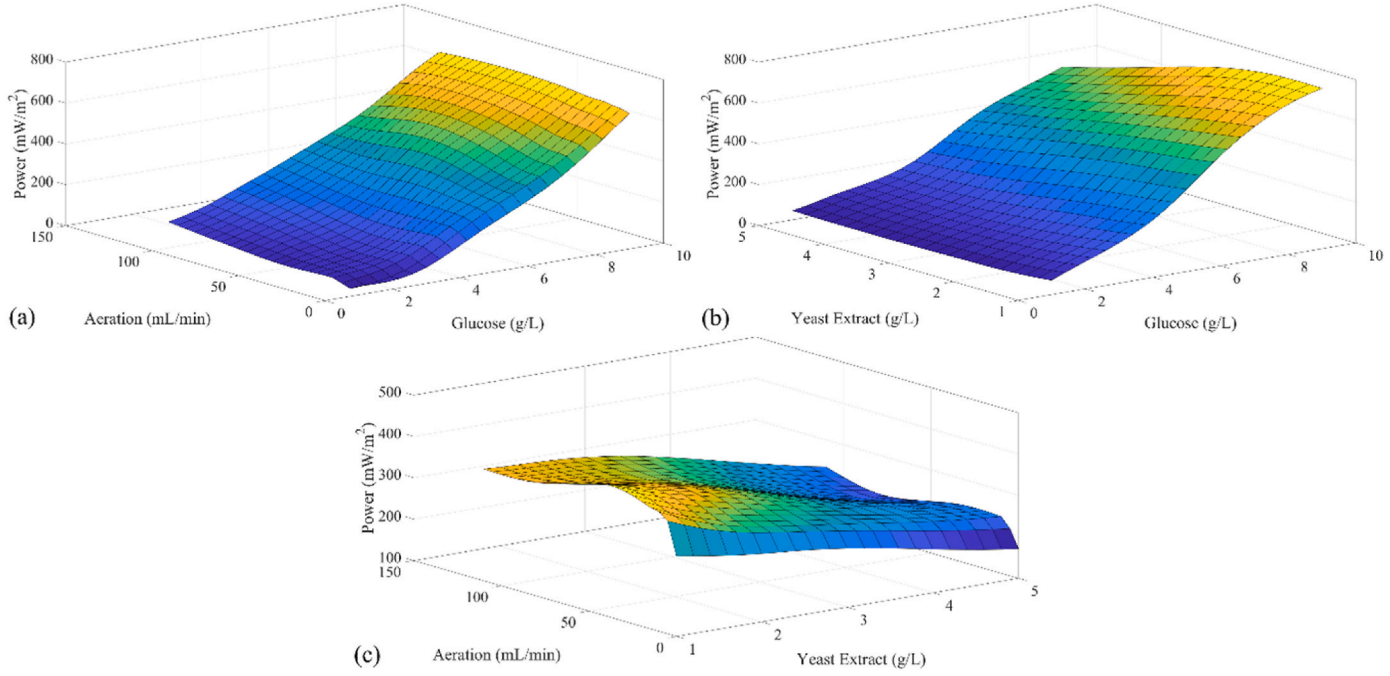

Fig. 9. P-GRU rule surface for calculation of power (mW/m^2) using (a) glucose-aeration; (b) glucose-yeast extract; (c) yeast extract-aeration.

and aeration (from 0 to 110 mL/min) with consideration of constant yeast extract (3 g/L). In addition, Fig. 8b shows the variation of COD removal based on the variation of glucose (from 0 to 10 g/L) and yeast extract (from 1 to 5 g/L) with consideration of constant aeration (55 mL/min). Also, Fig. 8c shows the variation of COD removal based on the variation of yeast extract (from 1 to 5 g/L) and aeration (from 0 to 110 mL/min) with consideration of constant glucose (5 g/L). In total, Fig. 8a and b show that increasing glucose normally increases COD removal. However, there is a local optimal point based on the amount of aeration and yeast extract. It proves the necessity of implementing the optimisation method in extracting the optimal solution of the process. Fig. 8b–c shows that the increasing yeast extract normally reduces the COD removal. However, there is a locally optimal point with a variation of the yeast extract, as observed in the glucose variation assessment. It is challenging to determine the influence of aeration on the variation in COD removal based on Fig. 8a and c. It demonstrates that aeration has the least influence on the variation in COD removal compared to glucose and yeast extract. However, some local optimal points should be extracted in the optimisation stage of the research.

Fig. 9a–c shows the rule surface of the extracted P-GRU in calculating power generation based on the arrangements of input process parameters, including glucose-aeration, glucose-yeast extract, and yeast extract-

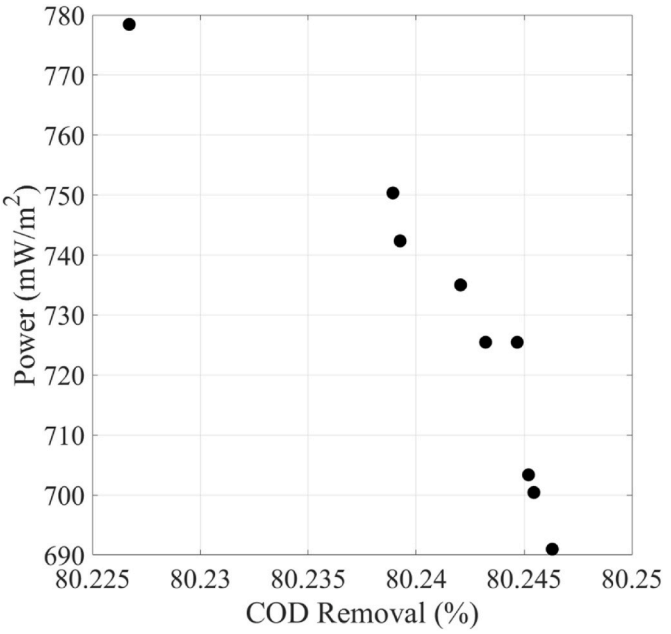

Fig. 10. Pareto front of the extracted optimal solution using MOO in the MFC process to extract the COD removal (%) and power (mW/m^2).

aeration, respectively. Fig. 9a presents the variation of power based on the variation of glucose (from 0 to 10 g/L) and aeration (from 0 to 110 mL/min) with consideration of constant yeast extract (3 g/L). In addition, Fig. 9b shows the variation of power based on the variation of glucose (from 0 to 10 g/L) and yeast extract (from 1 to 5 g/L) with consideration of constant aeration (55 mL/min). Also, Fig. 9c shows the variation of power based on the variation of yeast extract (from 1 to 5 g/L) and aeration (from 0 to 110 mL/min) with consideration of constant glucose (5 g/L). Fig. 9a–c shows that the system's behaviour in response to power variation, based on the different arrangements of glucose, yeast extract, and aeration, is simpler than that of COD removal compared to Fig. 9a–c. Fig. 9a and b demonstrate that the increase in glucose enhances the system's power generation. Additionally, Fig. 9 b and 9c show that the increase in yeast extract reduces power generation. Additionally, Fig. 9a and c demonstrate that the variation in aeration has a distinct influence on power, depending on the arrangement of glucose and yeast extract.

4.5. Optimisation

The two extracted models (COD-LSTM and P-GRU) are the objective functions of ISC inside the MOO using a genetic algorithm, investigated in Eqs. 29 and 30. Illustrated in Fig. 10 is the distribution of the optimal solution's Pareto front configuration within the context of the process. Moreover, the optimal solutions derived are outlined in Table 5. A sequence of MFC experiments was conducted to affirm the system's precision using the extracted optimal solution from the recently introduced approach. The margin of error between the experiment and predicted values of the 9 optimal recommended solutions via the investigated COD-LSTM and P-GRU methods is 7.64 % and 3.29 % on average for COD removal and power, respectively. It proves that COD-LSTM is less accurate than P-GRU. In addition, the lowest margin errors for COD-LSTM and P-GRU are captured during the 4th and 7th sets of the optimal solution, with 3.02 % and 0.97 %, respectively. The COD removal rate of 79.9 % achieved in this study is consistent with the findings of Ghasemi et al. [27], who reported similar efficiencies using optimised substrate concentrations. However, the integration of LSTM-based modelling in our approach enables more precise predictions and optimisation, resulting in a reduced margin of error compared to traditional methods. Additionally, the power generation efficiency of 767.9 mW/m^2 exceeds that reported by Nguyen et al. [28], highlighting the advantages of our GRU-based prediction model in addressing dynamic operational conditions.

The optimised solutions presented in this study are inherently scalable due to the modular design of MFC systems. By adjusting input parameters such as substrate type, operational conditions, and environmental variables, the proposed methodology can be adapted to meet region-specific requirements. For instance, locally available carbon and nitrogen sources can be substituted without compromising system performance in regions with limited access to glucose and yeast extract. Furthermore, climatic factors such as temperature and humidity, which influence microbial activity, can be integrated into the optimisation framework to enhance applicability across diverse geographies. Future research could focus on developing region-specific case studies to validate the scalability and adaptability of the proposed solutions.

4.6. Limitations of the study

Although the ISC-MOO framework showed encouraging results in enhancing MFC performance, several constraints must be recognised. Firstly, the experiments were conducted at a laboratory scale using a small reactor volume of 250 mL, which may limit the ability to scale up to full industrial applications without further pilot studies. Moreover, factors such as temperature variations, changes in the microbial community, and long-term operational stability were not thoroughly examined, which could influence system performance in practical scenarios. Regarding experimental precision, although steps were taken to minimise errors through repeated measurements and data processing, uncertainties in COD measurements due to sample matrix effects and spectrophotometer sensitivity may have led to some variations. Future research should aim to validate the models using different types of wastewaters, scale up the reactor system, and incorporate economic and environmental evaluations to enhance its wider applicability.

5. Conclusion

This study introduced a novel framework for optimising microbial fuel cells (MFCs) using a combination of deep learning models and a multi-objective genetic algorithm. Specifically, long short-term memory (LSTM) networks and gated recurrent units (GRU) were developed as

Table 5
Extracted optimal process parameters of the MFC process using the newly proposed models.

No.	G	YE	A	COD Exp	COD Pre	COD Error	P Exp	P Pre	P Error
1	9.0	1.68	21.38	69.7	80.23	15.11 %	739.1	778.42	5.32 %
2	8.8	2.36	12.20	74.3	80.24	7.99 %	734.7	725.44	1.26 %
3	8.7	2.46	12.19	77.8	80.25	3.15 %	729.6	703.34	3.60 %
4	8.6	2.55	12.08	77.9	80.25	**3.02 %**	747.2	690.96	7.53 %
5	8.8	2.32	12.55	74.5	80.24	7.70 %	752.3	734.99	2.30 %
6	8.8	2.14	13.21	72.6	80.24	10.52 %	776.8	742.34	4.44 %
7	8.6	2.49	12.18	79.9	80.25	4.40 %	693.7	700.41	**0.97 %**
8	8.8	2.39	12.57	74.6	80.24	7.56 %	739.4	725.45	1.89 %
9	8.9	2.17	13.68	79.5	80.24	9.30 %	767.9	750.32	2.29 %

surrogate models to predict chemical oxygen demand (COD) removal and power generation, respectively. These models were integrated into a multi-objective optimisation approach to identify optimal operational parameters.

Experimental validation of the Pareto-optimal solutions confirmed high accuracy, with prediction errors of 5.47 % for COD removal and 3.29 % for power output. The proposed method significantly reduces the need for extensive physical experimentation while maintaining reliability, thereby offering a scalable and cost-effective strategy for MFC system design.

Future research could explore the integration of economic and environmental impact indicators into the optimisation framework, as well as case-specific adaptation of the model to various regional wastewater compositions and operational conditions.

CRediT authorship contribution statement

Mohammad Reza Chalak Qazani: Writing – review & editing, Writing – original draft, Visualization, Validation, Software, Methodology, Investigation, Formal analysis, Conceptualization. **Mostafa Ghasemi:** Writing – review & editing, Writing – original draft, Resources, Investigation, Funding acquisition, Formal analysis, Data curation, Conceptualization. **Houshyar Asadi:** Writing – review & editing, Writing – original draft, Supervision, Software, Resources, Project administration, Conceptualization.

Data availability

Data will be made available on request.

Declaration of competing interest

The authors declare that they have no known competing financial interests or personal relationships that could have appeared to influence the work reported in this paper.

Acknowledgement

The authors gratefully acknowledge the financial support provided by the Yangtze Delta Region Institute, Huzhou of the University of Electronic Science and Technology of China (UESTC) through the Start-up Fund (Grant Number: U03220171).

Appendix A. Supplementary data

Supplementary data to this article can be found online at https://doi.org/10.1016/j.renene.2025.124188.

Appendix

Correlation coefficient (CC), mean square error (MSE), root mean square error (RMSE), and normalised root mean square error (NRMSE), mean of error, standard deviation (StD), and R-square (R^2) are employed to validate the investigated methods to choose the most reliable one. These validation parameters are calculated as follows:

$$CC = \frac{\sum_{i=1}^{n}(x_i - \overline{x})(T_i - \overline{T})}{\sqrt{\sum_{i=1}^{n}(x_i - \overline{x})^2 (T_i - \overline{T})^2}}$$

$$MSE = \frac{1}{n}\sum_{i=1}^{n}(T_i - \widehat{T}_i)^2$$

$$RMSE = \sqrt{\frac{\sum_{i=1}^{n}(T_i - \widehat{T}_i)^2}{n}}$$

$$NRMSE = \frac{RMSE}{\overline{T}}$$

$$Mean = \frac{1}{n}\sum_{i=1}^{n}(T_i - \widehat{T}_i)$$

$$StD = \sqrt{\frac{\sum_{i=1}^{n}(x_i - \overline{x})^2}{n}}$$

$$\mathbf{R^2} = \mathbf{1} - \frac{\sum_{i=1}^{n}(T_i - \widehat{T}_i)^2}{\sum_{i=1}^{n}(T_i - \overline{T})^2}$$

where n, x_i, $\overline{x}$ and $\overline{T}$ are the number of samples, the ith input, the mean of the inputs and the mean of outputs.

References

[1] A. Kadier, et al., A review of the substrates used in microbial electrolysis cells (MECs) for producing sustainable and clean hydrogen gas, Renew. Energy 71 (2014) 466–472.
[2] S.A. Saadabadi, et al., Solid oxide fuel cells fuelled with biogas: potential and constraints, Renew. Energy 134 (2019) 194–214.
[3] M.R.C. Qazani, M. Ghasemi, H. Asadi, Optimising microbial fuel cells with multiple-objectives PSO and type-2 fuzzy neural networks, Fuel 372 (2024) 132090.
[4] E. Elahi, Z. Khalid, Z. Zhang, Understanding farmers' intention and willingness to install renewable energy technology: a solution to reduce the environmental emissions of agriculture, Appl. Energy 309 (2022) 118459.
[5] E. Abdelsalam, et al., Dual-technology power plant as a potential solution for the clean water and electricity productions: Eritrea case study, Renew. Energy 201 (2022) 1050–1060.
[6] B. Steffen, A. Patt, A historical turning point? Early evidence on how the Russia-Ukraine war changes public support for clean energy policies, Energy Res. Social Sci. 91 (2022) 102758.
[7] L. Onwuemezie, H.G. Darabkhani, Biohydrogen production from solar and wind assisted AF-MEC coupled with MFC, PEM electrolysis of H2O and H2 fuel cell for small-scale applications, Renew. Energy (2024) 120160.
[8] R. Tamakloe, Effect of COD and H2O2 concentration on DC-MFC, Renew. Energy 83 (2015) 1299–1304.
[9] I. Sharafat, et al., Trivalent iron shaped the microbial community structure to enhance the electrochemical performance of microbial fuel cells inoculated with soil and sediment, J. Environ. Chem. Eng. 10 (3) (2022) 107790.
[10] M.A. Chowdhury, et al., Enhancement of microbial fuel cell performance by introducing dosing materials in waste water to increase microorganism growth, Renew. Energy 219 (2023) 119497.
[11] B. Ji, et al., Curbing per-and polyfluoroalkyl substances (PFASs): first investigation in a constructed wetland-microbial fuel cell system, Water Res. 230 (2023) 119530.
[12] Z. Ullah, Effect of catholyte on performance of photosynthetic microbial fuel cell for wastewater treatment and energy recovery, Renew. Energy 221 (2024) 119810.
[13] E.R. Ballestas, et al., Power generation potential of plant microbial fuel cells as a renewable energy source, Renew. Energy 221 (2024) 119799.
[14] Y. Yue, et al., Machine learning-based multi-performance prediction and analysis of Earth-Air Heat Exchanger, Renew. Energy 227 (2024) 120550.
[15] M.S. Timilsina, et al., Syngas composition analysis for waste to methanol production: techno-economic assessment using machine learning and Aspen plus, Renew. Energy 228 (2024) 120574.
[16] C. Zhao, et al., Prediction of bio-oil yield by machine learning model based on'enhanced data'training, Renew. Energy (2024) 120218.
[17] M.R.C. Qazani, et al., Multi-objective optimization of roll-forming procedure using NSGA-II and type-2 fuzzy neural network, IEEE Trans. Autom. Sci. Eng. 21 (3) (2023) 3842–3851.
[18] M.R.C. Qazani, et al., A machine learning method for cutting parameter selection in rotary ultrasonic-assisted end grinding, Int. J. Adv. Des. Manuf. Technol. (2023) 1–15.
[19] F. Fang, et al., Optimising multi-variables of microbial fuel cell for electricity generation with an integrated modeling and experimental approach, Appl. Energy 110 (2013) 98–103.
[20] A. Garg, et al., Performance evaluation of microbial fuel cell by artificial intelligence methods, Expert Syst. Appl. 41 (4) (2014) 1389–1399.
[21] K. Chen, S. Laghrouche, A. Djerdir, Degradation model of proton exchange membrane fuel cell based on a novel hybrid method, Appl. Energy 252 (2019) 113439.
[22] V. Kannan, et al., Quantifying operating uncertainties of a PEMFC–Monte Carlo-machine learning based approach, Renew. Energy 158 (2020) 343–359.
[23] K.A. Dwivedi, S.-J. Huang, C.-T. Wang, Integration of various technology-based approaches for enhancing the performance of microbial fuel cell technology: a review, Chemosphere 287 (2022) 132248.
[24] A. Coşgun, M.E. Günay, R. Yıldırım, Exploring the critical factors of algal biomass and lipid production for renewable fuel production by machine learning, Renew. Energy 163 (2021) 1299–1317.
[25] Y. Yang, et al., Biomass microwave pyrolysis characterisation by machine learning for sustainable rural biorefineries, Renew. Energy 201 (2022) 70–86.
[26] H. Shahbeik, et al., Characterising sludge pyrolysis by machine learning: towards sustainable bioenergy production from wastes, Renew. Energy 199 (2022) 1078–1092.
[27] M. Ghasemi, et al., Analysis and prediction of microbial fuel cell behaviour using MLP and SVR, J. Taiwan Inst. Chem. Eng. 151 (2023) 105101.
[28] D.D. Nguyen, et al., Guiding the optimisation of membraneless microfluidic fuel cells via explainable artificial intelligence: comparative analyses of multiple machine learning models and investigation of key operating parameters, Fuel 349 (2023) 128742.
[29] S.Z. Hossain, et al., Modeling of microbial fuel cell power generation using machine learning-based super learner algorithms, Fuel 349 (2023) 128646.
[30] G.A. Kebede, et al., Transfer learning-based deep learning models for proton exchange membrane fuel remaining useful life prediction, Fuel 367 (2024) 131461.
[31] J. Pan, et al., Machine learning optimisation for enhanced biomass-coal co-gasification, Renew. Energy (2024) 120772.
[32] M. Ghasemi, et al., Performance improvement of microbial fuel cell through artificial intelligence, Int. J. Energy Res. 45 (1) (2021) 342–354.
[33] M. Mohammadi, et al., Microbial fuel cell for oilfield produced water treatment and reuse: modelling and process optimisation, Kor. J. Chem. Eng. 38 (2021) 72–80.
[34] A.J. Myles, et al., An introduction to decision tree modeling, J. Chemometr.: J. Chem. Soc. 18 (6) (2004) 275–285.
[35] INVALID CITATION !!! [33-35].
[36] H. Yu, B.M. Wilamowski, Levenberg–marquardt training, in: Intelligent Systems, CRC Press, 2018, 12-1-12-16.
[37] K. Cho, et al., Learning phrase representations using RNN encoder-decoder for statistical machine translation, arXiv preprint arXiv:1406.1078 (2014).